Aircraft flight parameter estimation based on passive acoustic techniques using the polynomial Wigner–Ville distribution

David C. Reid,[a] Abdelhak M. Zoubir, and Boualem Boashash
Signal Processing Research Centre, Queensland University of Technology, G.P.O. Box 2434, Brisbane, Queensland 4001, Australia

(Received 15 May 1995; revised 25 January 1997; accepted 4 March 1997)

The acoustic signal from an overflying aircraft, as heard by a stationary observer, is used to estimate an aircraft's constant height, ground speed, range, and acoustic frequency. Central to the success of this flight parameter estimation scheme is the need for an accurate estimate of the instantaneous frequency of the observed acoustic signal. In this paper, the polynomial Wigner–Ville distribution is used in this application as the instantaneous frequency estimator. Its performance and the issue of the optimal time domain window length are addressed. © *1997 Acoustical Society of America.* [S0001-4966(97)06106-7]

PACS numbers: 43.28.Tc, 43.60.Gk [LCS]

INTRODUCTION

Ground-based radar systems are commonly used in military applications and general aviation to provide an estimate of an aircraft's height, ground speed, and range. In this paper we consider aspects of an alternative approach based on passive acoustic techniques which provide a simple, portable, easily implemented, covert, and biologically safe estimation scheme. In this scheme, the acoustic signal from an overflying aircraft is recorded by a single ground-based microphone. An estimate of the aircraft's flight parameters (constant height, constant ground speed, constant acoustic frequency, and range) can then be made by estimating the form of the time varying Doppler shift of the received acoustic signal.

The Doppler effect describes the perceived change in frequency of an acoustic source which is moving relative to an observer. The observed sound of an overflying aircraft provides a good example of this phenomenon. From experience, a stationary observer is able to make some useful judgement about the velocity and height of the overflying aircraft based on the observed time varying frequency of the narrow-band acoustic signal from the aircraft's engines or propellers. For example, a rapid transition in the acoustic frequency, as an aircraft passes overhead, would indicate to a stationary observer that the aircraft was either flying fast or low, or both. Ferguson[1] formalized this concept by proposing an observer frequency model which, based on a number of assumptions, relates the acoustic frequency of the observed signal to the aircraft flight parameters. The application of this model was demonstrated in Refs. 1 and 2 where it was shown that, given an estimate of the time varying acoustic frequency from a single microphone recording, the observer frequency model could be used to provide a meaningful estimate of the aircraft flight parameters. Central to the success of this passive acoustic parameter estimation scheme is the need for an accurate estimate of the aircraft's time varying acoustic frequency. In Ref. 3 it is shown that this acoustic frequency is the instantaneous frequency of the observed passive acoustic signal.

In Sec. I we discuss the use of time–frequency representations (TFRs) as instantaneous frequency estimators. In particular we briefly compare the use of the polynomial Wigner–Ville distribution and the Wigner–Ville distribution.[4,2,5] Other estimation schemes have been proposed based on spectral phase,[1,6] central finite difference and signal phase estimators,[3,7] and frequency and signal amplitude.[8] Bootstrap statistical techniques have been employed to determine confidence bounds for the aircraft parameters given a single acoustic recording.[9,7] A general discussion of the aircraft flight parameter estimation scheme is presented in Sec. II where examples of the passive acoustic instantaneous frequency and its relationship to the flight parameters is given. In Sec. III it is shown that a trade-off between the bias and variance of the polynomial Wigner–Ville and Wigner–Ville based instantaneous frequency estimators can be controlled by using a time domain window. Comparative examples of this trade-off are given for these time–frequency representations and analytical expressions for the instantaneous frequency estimator bias and variance and optimal window length are derived. These theoretical results are supported by computer simulations in Sec. IV and the strengths and limitations of the polynomial Wigner–Ville distribution in the passive acoustic application are demonstrated.

I. INSTANTANEOUS FREQUENCY ESTIMATION

The acoustic signal from a propeller driven aircraft is narrow-band with the dominant frequency given by the propeller blade rate which is defined as the product of the engine rotational speed and the number of propeller blades.[1] The aircraft acoustic signal, as heard by a stationary observer is nonstationary in the sense that the spectral content varies with time due to the Doppler effect. Consideration of the frequency of such acoustic signals, at a particular time instant, leads to the concept of instantaneous frequency (see Ref. 10 for a detailed discussion of instantaneous frequency). One particular method of instantaneous frequency estimation

[a]Commonwealth Scientific and Industrial Research Organisation, Exploration and Mining, Queensland Centre for Advanced Technologies, P.O. Box 883, Kenmore, Queensland 4069, Australia.

is based on the signal's time–frequency representation. The time–frequency representation is a two-dimensional function which attempts to show the distribution of the signal energy in a joint time–frequency plane. Ideally we would like all the energy concentrated at the instantaneous frequency, denoted $f_i(t)$, so as to yield the ideal time–frequency representation

$$\mathcal{T}(t,f) \propto (\delta[f - f_i(t)]), \tag{1}$$

where $\delta(.)$ is the Dirac delta and $\propto$ indicates proportionality. It follows that the peak of (1) would describe $f_i(t)$ exactly. In practice, due to finite data lengths, noisy observations, and the particular characteristics of the time–frequency representation being used, we only obtain an approximation to (1). For a particular signal, some time–frequency representations will provide a better approximation than others. For example, the Wigner–Ville distribution is optimal for the analysis of deterministic signals having a linearly time varying instantaneous frequency law.

For this class of signals, the peak of the Wigner–Ville distribution, with respect to time, describes exactly the instantaneous frequency. In a similar manner, the peak of a class of time–frequency representations known as polynomial Wigner–Ville distributions provide an optimal instantaneous frequency estimate for deterministic signals having an instantaneous frequency not exceeding a given polynomial order.[11]

II. THE AIRCRAFT FLIGHT PARAMETER ESTIMATION SCHEME

A. The observer frequency model

The passive acoustic observer frequency model proposed in Ref. 1 is based on the assumptions that, throughout the observation period: (1) the aircraft is flying at a constant altitude and subsonic ground speed, (2) the wind velocity is constant in both space and time, and (3) the acoustic source frequency is constant. These assumptions only need to hold throughout the observation period (typically about 30 s). Under these assumptions, the observer frequency model, $f_0(t)$, is given by

$$f_0(t) = \frac{f_a(c + v_m \cos\ \gamma(t))}{(c + v_m \cos\ \gamma(t) \pm v_a \cos\ \gamma(t))}, \tag{2}$$

where f_a is the source acoustic frequency, c is the speed of sound in the medium, v_m is the velocity of the wind, and v_a is the velocity of the aircraft, where each velocity represents the component along the aircraft flight path. Furthermore, $\gamma(t)$ is the angle of depression of the observer from the aircraft such that

$$\cos\ \gamma(t) = \frac{r(t)}{\sqrt{h^2 + r^2(t)}}, \tag{3}$$

where h is the distance between the aircraft and the observer at the point of closest approach, and $r(t)$ is the horizontal range of the aircraft from the observer when it generates the sound that reaches the observer later at time t, which is defined to be

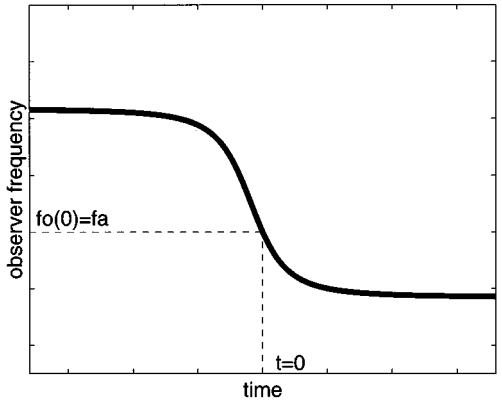

FIG. 1. The general form of the passive acoustic instantaneous frequency as described by the observer frequency model. The intersection of the dashed lines indicates the time in the instantaneous frequency where the acoustic signal from the directly overhead aircraft is subsequently heard by the observer.

$$t = \frac{\pm r(t)}{v_a} + \frac{\sqrt{(h^2 + r^2(t))} - h}{c}. \tag{4}$$

If the flight path of the aircraft is directly over the observer (i.e., overflying), h is the constant height of the aircraft above the observer. Experimental results with real aircraft acoustic data, collected under accurately monitored conditions, have confirmed the veracity and practical usefulness of the observer frequency model.[3]

The general form of the observer frequency model $f_0(t)$ is shown qualitatively in Fig. 1. The intersection of the dashed lines is the value of the instantaneous frequency where the acoustic signal from the aircraft at the point of closest approach (i.e., no Doppler shift) is subsequently heard by the observer. At this point $t=0$, $r(0)=0$, and $f_0(0)=f_a$. A more detailed description of this model can be found in Ref. 1. Given v_m and c, the aircraft flight parameters which are to be estimated, v_a, h, $r(t)$, and f_a are uniquely related to $f_0(t)$ by (2). It is for this reason that we now turn our attention to the estimation of $f_0(t)$.

B. Passive acoustic instantaneous frequency estimation

In Refs. 2 and 4 the Wigner–Ville distribution was used in the aircraft flight parameter estimation application. An example of this technique is given in Fig. 2 which shows the Wigner–Ville distribution of an acoustic recording of an overlying propeller-driven light aircraft being flown under controlled conditions. The form of the instantaneous frequency is graphically evident and indicates that the peak of this time–frequency representation provides an estimate of the instantaneous frequency. Such an estimate is given in Fig. 3.

The polynomial Wigner–Ville distribution, which will be defined and described in detail in Sec. III, is a class of time–frequency representations which include and extend the Wigner–Ville distribution to higher polynomial orders. For the purpose of comparison, Fig. 4 shows the fourth-order polynomial Wigner–Ville distribution of the same acoustic

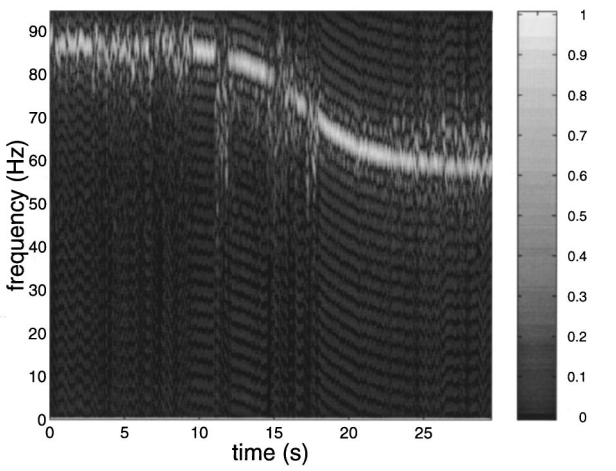

FIG. 2. A Wigner–Ville time–frequency representation of a typical acoustic recording of an overflying aircraft.

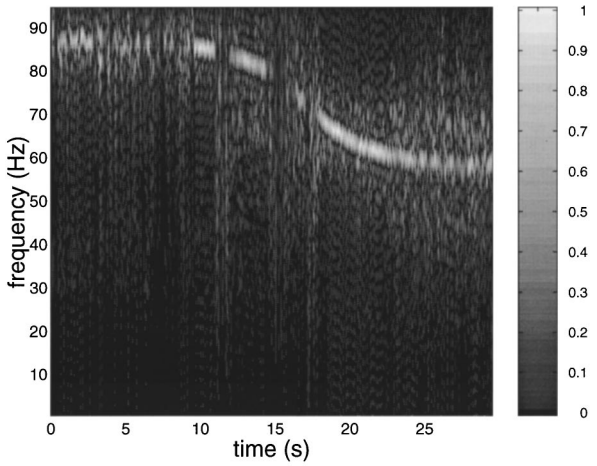

FIG. 4. A fourth-order polynomial Wigner–Ville time–frequency representation of the same acoustic recording as used in Fig. 2.

signal as used in Fig. 2 and the corresponding instantaneous frequency estimate is shown in Fig. 5. It is apparent that the Wigner–Ville- and polynomial Wigner–Ville-based instantaneous frequency estimates of Fig. 3 and 5 differ from each other. The noticeable differences are that the polynomial Wigner–Ville-based estimator has higher variance at the extremities which corresponds to the distant aircraft and consequently is the region of low signal-to-noise ratio. Also the Wigner–Ville-based estimator performs poorly in the central transitional region where the coefficients of the higher-order derivatives of instantaneous frequency, with respect to time, are greatest. These observations are significant as it will be shown in later sections that the choice between the Wigner–Ville and polynomial Wigner–Ville as an instantaneous frequency estimator is, in general, very much dependent on the signal-to-noise ratio and the higher-order derivatives present in the instantaneous frequency law.

In this particular application, the aircraft flight parameters being estimated are a nonlinear function of the instantaneous frequency. Each of the parameters depend, to a varying extent, on different temporal regions or characteristics of the observer frequency model. For example, the height parameter is particularly sensitive to the form of the central transitional region of the frequency model, whereas the source frequency parameter is largely dependent on the flat extremities, and by comparison with the height parameter, is far less sensitive. This dependence is demonstrated graphically in Fig. 6 where the solid line represents $f_0(t)$ for typical parameters: $h=304.8$ m (1000 ft), $v_a=102.9$ m/s (200 kn), $f_a=100$ Hz, and at an arbitrarily chosen time reference, $r=1.646$ km. For the instantaneous frequency described by the dashed line, the relatively small change in the central transitional region results from a 50% reduction in the value of the height parameter with the other parameters remaining unchanged. On the other hand, the instantaneous frequency described by the dotted line results from only a 5% reduction in the source frequency parameter with the other parameters remaining unchanged.

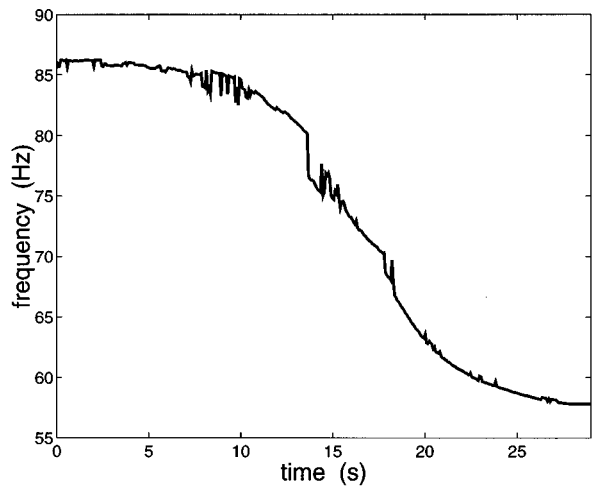

FIG. 3. An instantaneous frequency estimate given by the peak, with respect to time, of the Wigner–Ville time–frequency representation of Fig. 2.

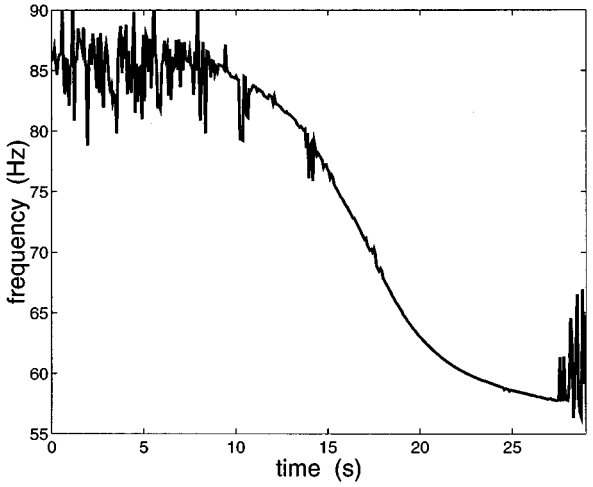

FIG. 5. An instantaneous frequency estimate given by the peak, with respect to time, of the fourth-order polynomial Wigner–Ville time–frequency representation of Fig. 4.

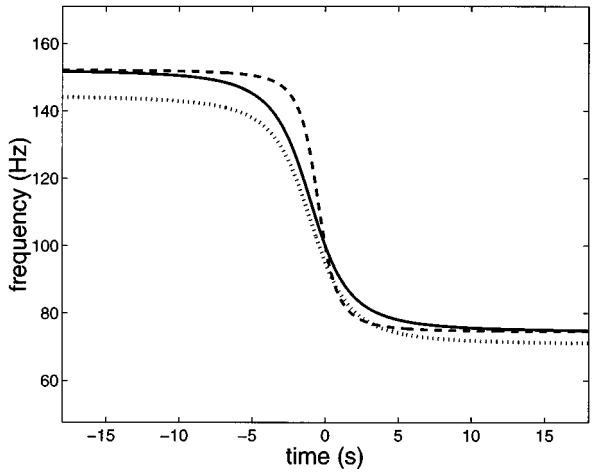

FIG. 6. A comparison of the instantaneous frequency, as described by the observer frequency model, for varying values of the height and source frequency parameter. The aircraft flight parameters associated with the solid line are $h=304.8$ m (1000 ft), $v_a=102.9$ m/s (200 kn), $f_a=100$ Hz and range=1.646 km. The dashed line is the instantaneous frequency where the height parameter alone has been reduced by 50% and the dotted line is the instantaneous frequency where the source frequency parameter alone has been reduced by 5%.

C. Aircraft flight parameter estimates

In the final step in this flight parameter estimation scheme we extract the parameters by fitting the instantaneous frequency estimate to the observer frequency model in a minimum least-squares sense. Using this approach, the aircraft parameter estimates, based on the Wigner–Ville and fourth-order polynomial Wigner–Ville derived instantaneous frequency estimates of Figs. 3 and 5, respectively, are shown in Table I (for this example we have used $c=339$ m/s, $v_m=0$ and have calculated the range corresponding to $t=0$ s).

In the remaining sections we consider the use of the Wigner–Ville distribution and polynomial Wigner–Ville distribution as estimators of higher polynomial order instantaneous frequency laws (such as the passive acoustic instantaneous frequency).

III. THE POLYNOMIAL WIGNER–VILLE DISTRIBUTION

A desirable property of a time–frequency representation is that it provides good concentration by localizing the signal energy in both time and frequency. Numerous time–frequency representations have been proposed that exhibit this property for particular classes of signals, achieving both good time and frequency concentration simultaneously.[12] Significant among these is the Wigner–Ville distribution which is known, for linear frequency modulated signals (i.e., linear instantaneous frequency), to be an ideal time–frequency representation in that it provides maximum localization of the signal energy about the true instantaneous frequency. The instantaneous frequency $f_i(t)$ of a real valued signal $x(t)$ can be expressed as

$$f_i(t)=\frac{1}{2\pi}\frac{d\theta(t)}{dt}, \tag{5}$$

where $\theta(t)$ is the phase of the analytic signal associated with $x(t)$.[10] From (5), it follows that a linear or first-order polynomial frequency law corresponds to a second-order polynomial phase law. For polynomial phase laws greater than two, the Wigner–Ville distribution will become distorted and the peak of the time–frequency representation will no longer exactly describe the instantaneous frequency.[13] Polynomial Wigner–Ville distributions are a higher order extension of the Wigner–Ville distribution and are designed to properly localize, in time and frequency, signals having higher-order instantaneous frequency laws.[11] The qth-order polynomial Wigner–Ville distribution (which we abbreviate as PWVD$_q$) will provide an optimal time–frequency representation of a signal having phase law of polynomial order $\leqslant q$, in which case we say that the polynomial Wigner–Ville distribution and the signal are matched (the Wigner–Ville distribution is the second-order polynomial Wigner–Ville distribution).

TABLE I. Comparison of aircraft flight parameter estimates using the Wigner–Ville and polynomial Wigner–Ville distribution.

	Height (m)	Velocity (m/s)	Range (km)	Source freq. (Hz)
WVD	404	73.3	1.30	68.4
PWVD	309	68.7	1.21	68.9

A. Definitions

The qth-order polynomial Wigner–Ville distribution, denoted as $W_q(t,f)$, is defined in terms of the Fourier transform of a qth-order kernel function $K_q(t,f)$. With the inclusion of a time domain window, which controls the trade-off between estimator bias and variance, the qth-order polynomial Wigner–Ville distribution is defined as[14]

$$W_q(t,f)\triangleq\int_{-\infty}^{\infty}h(\tau)K_q(t,\tau)e^{-j2\pi f\tau}\,d\tau, \tag{6}$$

where

$$K_q(t,\tau)\triangleq\prod_{k=0}^{q/2}z(t+c_k\tau)^{b_k}z^*(t+c_{-k}\tau)^{-b_{-k}}, \tag{7}$$

$z(t)$ is the analytic signal associated with $x(t)$ and, for our purposes, we choose $h(\tau)$ to be a centered rectangular window function of length T. In the ''integer power'' implementation of the polynomial Wigner–Ville distribution[15] that we are considering, b_k is an integer, $b_k=-b_{-k}$, $q/2$ is a positive integer, c_k is a real number, and $c_k=-c_{-k}$. As discussed in Refs. 15 and 11, the values of b_k and c_k are chosen so that for each time increment, the kernel $K_q(t,\tau)$ attempts to demodulate $z(t)$ into a complex sinusoid with frequency equal to the instantaneous frequency. If this is achieved (and as T increases) the resulting time–frequency representation $W_q(t,f)$ approaches $\mathcal{T}(t,f)$ by exhibiting impulses in the time–frequency plane at coordinates corresponding to the true instantaneous frequency. The set of b_k coefficients are uniquely specified by further requiring that $\Sigma_k|b_k|$ be minimized. This requirement minimizes the number of multiplicative terms, and therefore the multilinearity, of the kernel.

For the specific case of the fourth-order polynomial Wigner–Ville, the kernel parameters are[15]

$$b_2=-b_{-2}=1, \quad b_1=-b_{-1}=2, \quad b_0=0, \tag{8}$$

$$c_1=-c_{-1}=\frac{1}{2(2-2^{1/3})}\approx 0.675, \quad c_2=-c_{-2}=-2^{1/3}c_1\approx -0.85. \tag{9}$$

For $k=0$, $z(t+c_{\pm 0})=1$ for all values of $c_{\pm 0}$ so that c_0 or $-c_{-0}$ need not be specified.

These parameter values yield the fourth-order kernel

$$K_4(t,\tau)=[z(t+0.675\tau)z^*(t-0.675\tau)]^2 \times z^*(t+0.85\tau)z(t-0.85\tau). \tag{10}$$

Similarly, for the second-order case,

$$b_1=-b_{-1}=1, \quad b_0=0, \tag{11}$$

$$c_1=-c_{-1}=0.5 \tag{12}$$

yielding the second-order kernel

$$K_2(t,\tau)=z(t+0.5\tau)z^*(t-0.5\tau) \tag{13}$$

which results in the Wigner–Ville distribution.

The purpose of the window function $h(\tau)$ is discussed next.

B. Time domain window effect on instantaneous frequency estimator error

In the absence of noise, exact instantaneous frequency estimates up to polynomial order $(q-1)$ can be obtained from the peak of the qth-order polynomial Wigner–Ville distribution, however, error in the instantaneous frequency estimates occurs when analyzing signals having polynomial phase laws of order greater than q. Furthermore, it will be shown that, for a given polynomial phase law of order p such that $p>q$, this instantaneous frequency error will increase as q decreases. It is this error, which manifests itself in the absence of noise, that we will refer to as systematic bias. This systematic bias may be minimized by using a time domain window to provide a region of time support where the signal's polynomial phase law can be locally approximated as qth order. It will be shown that the systematic bias *decreases* with decreasing window length.

In the presence of noise, there is also an error due to the variance of the estimator. It will be shown that the variance, which of course increases with decreasing signal-to-noise ratio, also *decreases* with increasing window length. Thus the two instantaneous frequency error factors behave in a counterdependent manner over window length. The effect of the time domain window is illustrated below by example using simulated signals.

In the following examples we use the discrete fourth-order polynomial Wigner–Ville distribution and Wigner–Ville distribution to analyze a seventh-order polynomial phase test signal $z(t)$. This test signal is intentionally chosen to be of higher polynomial order than the time–frequency representations so as to ensure that the signal is mismatched and that the effects of time domain windowing can be observed. The test signal is given by

$$z(t)=e^{j2\pi\phi(t)}+n(t), \quad t=-N/2+1,\ldots,N/2-1, \tag{14}$$

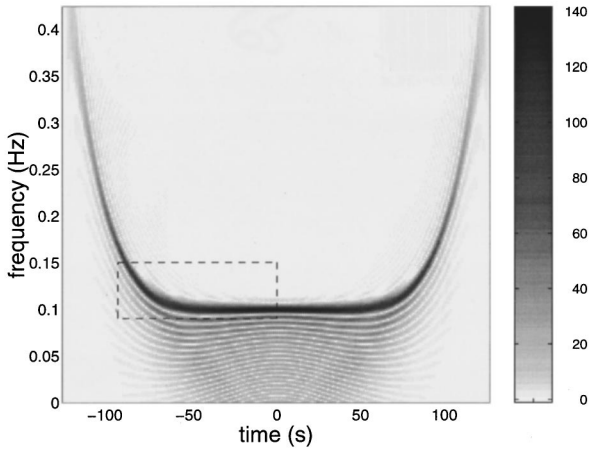

FIG. 7. A fourth-order polynomial Wigner–Ville distribution of a seventh-order polynomial phase test signal at 40-dB signal-to-noise ratio, where a long window (100% of data length) has been used. The dashed rectangular box marks the region in which the instantaneous frequency estimate comparison of Fig. 9 is made.

$$\phi(t)=0.1t+0.4t^7/(7(N/2)^6), \tag{15}$$

t is an integer, $n(t)$ is a complex white Gaussian stationary noise process, and $N=256$. By the definition of instantaneous frequency in (5), $z(t)$ represents a sixth-order frequency modulated signal with a maximum and a minimum frequency of 0.5 and 0.1 Hz, respectively.

1. Example 1

The fourth-order polynomial Wigner–Ville distribution and Wigner–Ville distribution of $z(t)$ at 40-dB signal-to-noise ratio, where a long window (100% of data length) has been used, are shown in Figs. 7 and 8, respectively. An instantaneous frequency estimate, based on the clearly distinguishable peaks of these time-frequency representations, will exhibit low variance but will be distorted away from the true instantaneous frequency. This distortion, which is due to the systematic bias, is shown in Fig. 9 where an enlarged portion

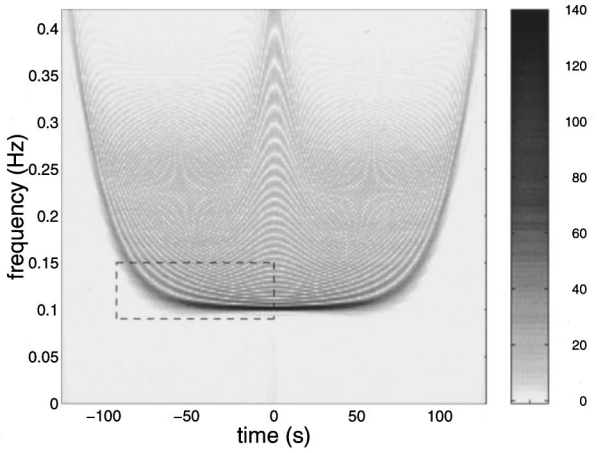

FIG. 8. A Wigner–Ville distribution (second-order polynomial Wigner–Ville distribution) of a seventh-order polynomial phase test signal at 40-dB signal-to-noise ratio, where a long window (100% of data length) has been used. The dashed rectangular box marks the region in which the instantaneous frequency estimate comparison of Fig. 9 is made.

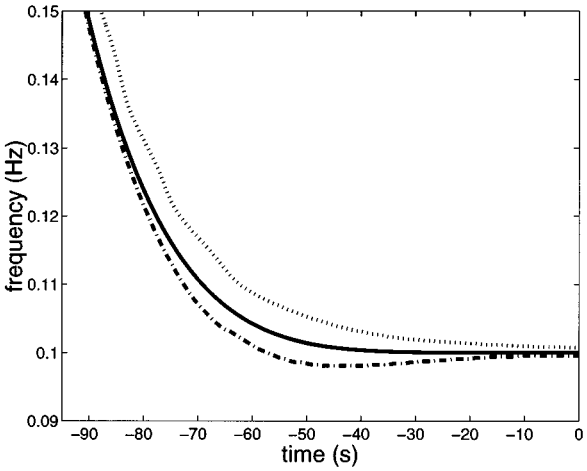

FIG. 9. An enlarged portion of the true instantaneous frequency (solid line) is compared to the instantaneous frequency estimates based on the peak of the fourth-order polynomial Wigner–Ville distribution (dashed line) of Fig. 7 and the Wigner–Ville distribution (dotted line) of Fig. 8 in the regions marked by the dashed rectangular boxes. The maximum systematic error occurs in this portion of the instantaneous frequency estimate. The mean-square error of the fourth-order polynomial Wigner–Ville-based estimate is approximately one-tenth that of the Wigner–Ville based estimate.

of the true instantaneous frequency (solid line) is compared to the instantaneous frequency estimates based on the peak of the fourth-order polynomial Wigner–Ville distribution (dashed line) and Wigner–Ville distribution (dotted line) of Figs. 7 and 8, respectively, in the region marked by the dashed rectangular box. In this case, the instantaneous frequency estimator mean-square error is essentially that associated with the systematic bias. Furthermore, the mean-square error of the fourth-order polynomial Wigner–Ville based estimate (which for this realization is estimated to be 4.2×10^{-6} Hz^2) is much less than for the Wigner–Ville based estimate (which is estimated for this realization to be 3.5×10^{-5} Hz^2). For a short window (3% of data length), the fourth-order polynomial Wigner–Ville and Wigner–Ville distribution, as shown in Figs. 10 and 11, respectively, are smeared in frequency and the peaks are of lower amplitude and are not so clearly distinguishable. However, the systematic bias has been reduced, as shown in Fig. 12, where the true instantaneous frequency and the estimates are practically coincident, and the mean-square error associated with the systematic bias of both estimates is negligible. In the high signal-to-noise ratio case, the short window estimate of Fig. 12 will give the more accurate instantaneous frequency estimate for both the polynomial Wigner–Ville distribution and the Wigner–Ville distribution, even though the peaks of both time-frequency representations are indistinct and of a much lower amplitude than for the large window time–frequency representations of Figs. 7 and 8.

2. Example 2

We now consider the same instantaneous frequency estimates of example 1 in the presence of noise at 10-dB signal-to-noise ratio. Figures 13 and 14 show the fourth-order polynomial Wigner–Ville distribution and Wigner–Ville distribution, respectively, of the noisy signal when a

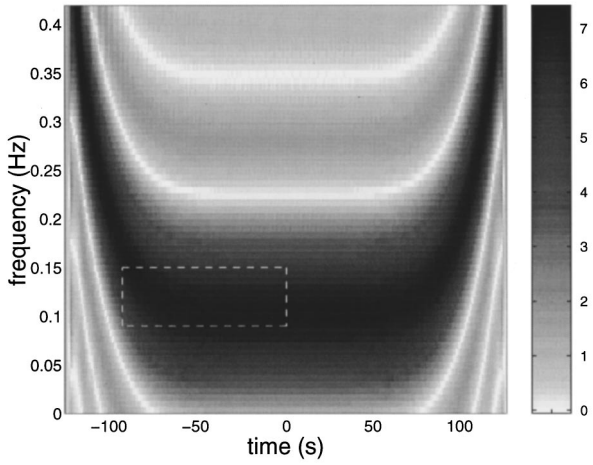

FIG. 10. A fourth-order polynomial Wigner–Ville distribution of a seventh-order polynomial phase test signal at 40-dB signal-to-noise ratio, where a short window (3% of data length) has been used. The dashed rectangular box marks the region in which the instantaneous frequency estimate comparison of Fig. 12 is made.

full length window is used. It appears that the peak of both time–frequency representations are still clearly distinguishable and that the overall instantaneous frequency estimator mean-square error will still essentially be that associated with the systematic bias. This is confirmed in Fig. 15 which shows a comparison of the true instantaneous frequency (solid line) and instantaneous frequency estimates based on the fourth-order polynomial Wigner–Ville distribution (dashed line) and Wigner–Ville distribution (dotted line) of Figs. 13 and 14, respectively, in the region marked by the dashed rectangular box. The mean-square error for the fourth-order polynomial Wigner-Ville- and Wigner–Ville-based estimates are 4.5×10^{-6} Hz^2 and 4.2×10^{-5} Hz^2, respectively, and are essentially the same as for the high signal-to-noise ratio example of Fig. 9. Figures 16 and 17 show the fourth-order polynomial Wigner–Ville and Wigner–Ville distribution of the noisy signal when the short

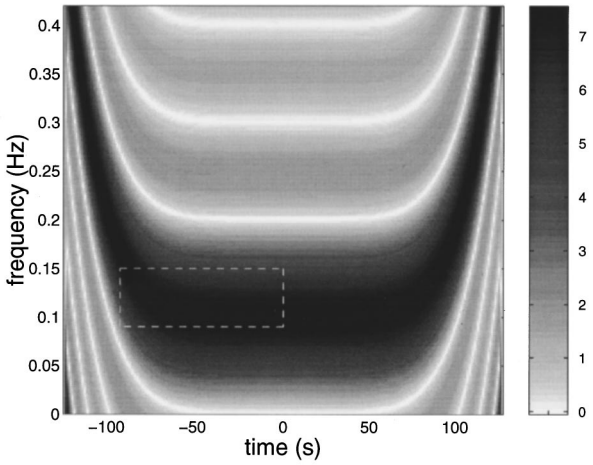

FIG. 11. A Wigner–Ville distribution (second-order polynomial Wigner–Ville distribution) of a seventh-order polynomial phase test signal at 40-dB signal-to-noise ratio, where a short window (3% of data length) has been used. The dashed rectangular box marks the region in which the instantaneous frequency estimate comparison of Fig. 12 is made.

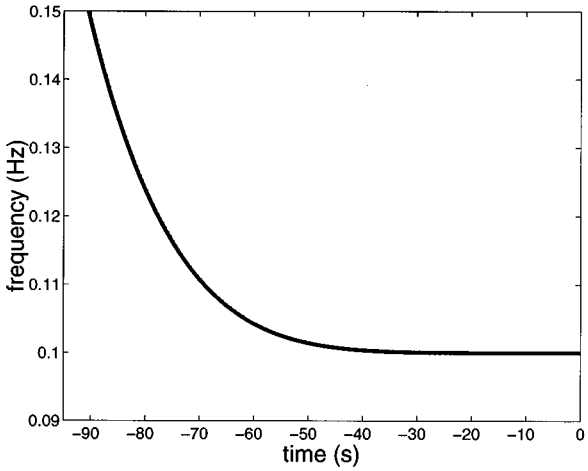

FIG. 12. An enlarged portion of the true instantaneous frequency (solid line) is compared to the instantaneous frequency estimates based on the peak of the fourth-order polynomial Wigner–Ville distribution of Fig. 10 and the Wigner–Ville distribution of Fig. 11 in the regions marked by the dashed rectangular boxes. In this plot, the three lines are coincident and the systematic error, which is maximum in this region, is negligible for both time–frequency representations.

window is used. Figure 18 shows the comparison of the true instantaneous frequency (heavy solid line), fourth-order polynomial Wigner–Ville-based estimate (broken line) and Wigner–Ville-based estimate (finer solid line) for a single realization. It is apparent that the mean-square error of the fourth-order polynomial Wigner–Ville-based estimator (calculated for this realization to be 3.3×10^{-5} Hz^2) will be greater than the Wigner–Ville-based estimator (calculated for this realization to be 9.3×10^{-6} Hz^2). It is also apparent that the mean-square error for both of these estimators, which are dominated by the estimator variance, may be greater than for the long window case of Fig. 15.

These simple examples demonstrate the relationship between instantaneous frequency estimator error, signal-to-noise ratio, window length, and the polynomial phase order

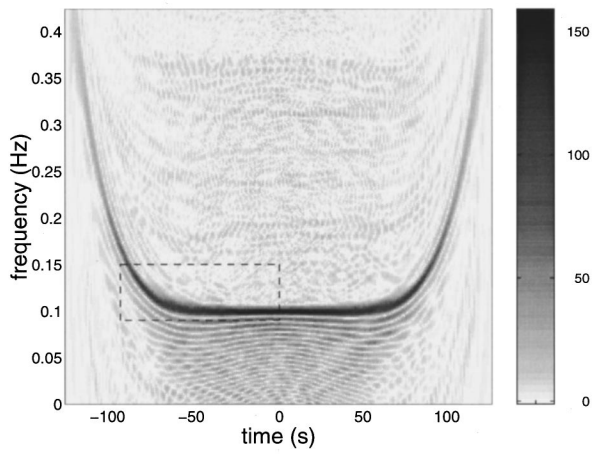

FIG. 13. A fourth-order polynomial Wigner–Ville distribution of a seventh-order polynomial phase test signal at 10-dB signal-to-noise ratio, where a long window (100% of data length) has been used. The dashed rectangular box marks the region in which the instantaneous frequency estimate comparison of Fig. 15 is made.

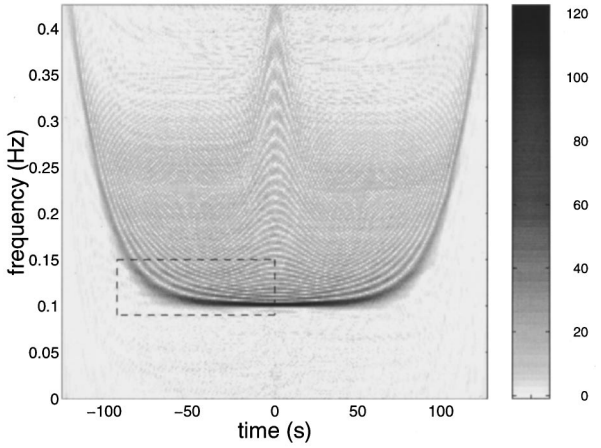

FIG. 14. A Wigner–Ville distribution (second-order polynomial Wigner–Ville distribution) of a seventh-order polynomial phase test signal at 10-dB signal-to-noise ratio, where a long window (100% of data length) has been used. The dashed rectangular box marks the region in which the instantaneous frequency estimate comparison of Fig. 15 is made.

of the signal. In the following sections we formalize these relationships by deriving expressions for the bias and variance of the polynomial Wigner–Ville-based instantaneous frequency estimator as functions, amongst other things, of the time domain window length. An expression for the optimal window length for the qth-order polynomial Wigner–Ville distribution is then derived where the criterion of optimality is the instantaneous frequency estimator minimum mean-square error. The derivations presented in the paper extend and generalize the fourth-order results previously presented in Ref. 16.

C. Polynomial Wigner–Ville-based instantaneous frequency estimator bias

We first consider the bias of the polynomial Wigner–Ville-based instantaneous frequency estimator which is com-

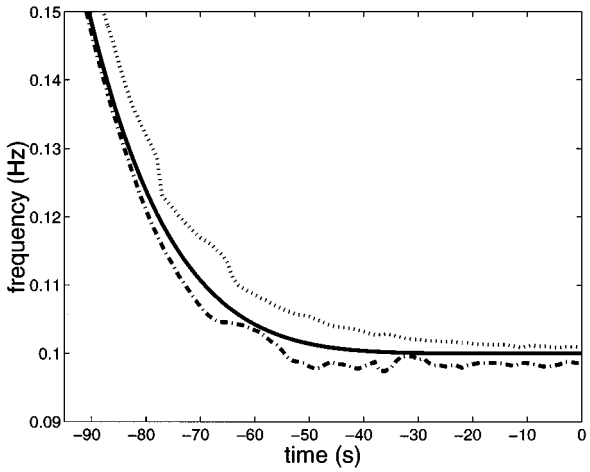

FIG. 15. An enlarged portion of the true instantaneous frequency (solid line) is compared to the instantaneous frequency estimates based on the peak of the fourth-order polynomial Wigner–Ville distribution (dashed line) of Fig. 13 and the Wigner–Ville distribution (dotted line) of Fig. 14 in the regions marked by the dashed rectangular boxes. The maximum systematic error occurs in this portion of the instantaneous frequency estimate.

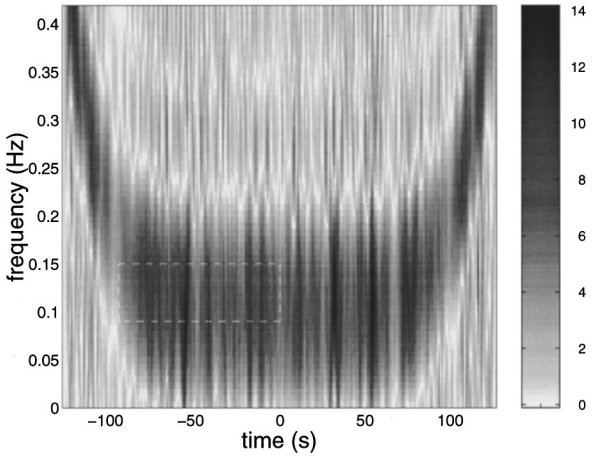

FIG. 16. A fourth-order polynomial Wigner–Ville distribution of a seventh-order polynomial phase test signal at 10-dB signal-to-noise ratio, where a short window (3% of data length) has been used. The dashed rectangular box marks the region in which the instantaneous frequency estimate comparison of Fig. 18 is made.

posed of two parts: the statistical bias (due to random effects), and the systematic bias (due to model mismatch). For the high signal-to-noise ratio case, which we consider in the following derivation, the statistical bias is considered to be negligible[17] and only the systematic bias, which results solely from the mismatched polynomial order of the polynomial Wigner–Ville distribution and the signal phase law, is of concern. An expression for the bias of the qth-order polynomial Wigner–Ville distribution can be derived as follows.

Consider a complex signal of the form

$$s(t)=Ae^{j2\pi\phi(t)}, \tag{16}$$

where t is a real number and where $\phi(t)$ is described, at least within some observation window, by a polynomial phase law of arbitrary order p. Expanding the qth-order kernel in (7) for this signal results in the phase terms

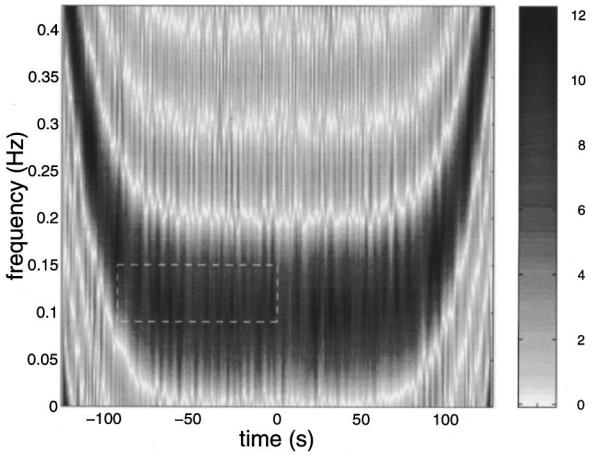

FIG. 17. A Wigner–Ville distribution (second-order polynomial Wigner–Ville distribution) of a seventh-order polynomial phase test signal at 10-dB signal-to-noise ratio, where a short window (3% of data length) has been used. The dashed rectangular box marks the region in which the instantaneous frequency estimate comparison of Fig. 18 is made.

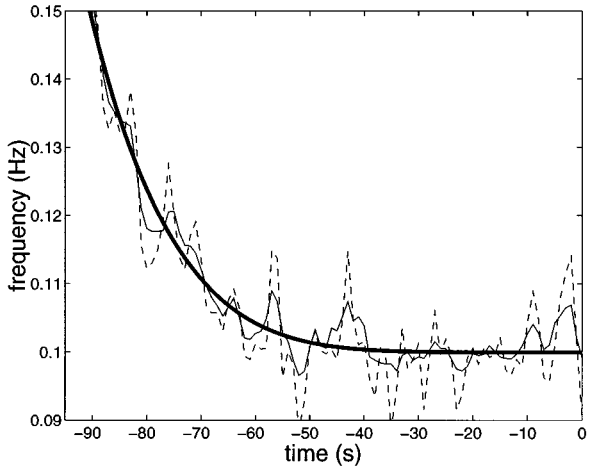

FIG. 18. An enlarged portion of the true instantaneous frequency (heavy solid line) is compared to the instantaneous frequency estimates based on the peak of the fourth-order polynomial Wigner–Ville distribution (dashed line) of Fig. 16 and Wigner–Ville distribution (finer solid line) of Fig. 17 in the regions marked by the dashed rectangular boxes. The mean-square error of both estimates is dominated by the estimator variance. The mean-square error of the fourth-order polynomial Wigner–Ville based estimate is approximately three times that of the Wigner–Ville based estimate.

$$\arg K_q[s(t)]=2\pi\sum_{k=-q/2}^{q/2} b_k\phi(t+c_k\tau). \tag{17}$$

By Taylor series expansion about an arbitrary point t, an exact expression for the kernel phase of $s(t)$ is:

$$\begin{aligned}
&\arg K_q[s(t)]\\
&=2\pi\Bigg[\frac{d\phi(t)}{dt}\,\tau+\frac{\tau^{(q+1)}}{(q+1)!}\,\frac{d^{(q+1)}\phi(t)}{dt^{(q+1)}}\sum_{k=-q/2}^{q/2} b_k c_k^{(q+1)}\\
&\quad+\frac{\tau^{(q+3)}}{(q+3)!}\,\frac{d^{(q+3)}\phi(t)}{dt^{(q+3)}}\\
&\quad\times\sum_{k=-q/2}^{q/2} b_k c_k^{(q+3)}+\cdots+\frac{\tau^p}{p!}\,\frac{d^p\phi(t)}{dt^p}\sum_{k=-q/2}^{q/2} b_k c_k^p\Bigg]\\
&=2\pi\Bigg[\frac{d\phi(t)}{dt}\,\tau+\sum_{l=q/2}^{(p-1)/2}\frac{\tau^{(2l+1)}}{(2l+1)!}\,\frac{d^{(2l+1)}\phi(t)}{dt^{(2l+1)}}\\
&\quad\times\sum_{k=-q/2}^{q/2} b_k c_k^{(2l+1)}\Bigg]\\
&=2\pi\Bigg[\frac{d\phi(t)}{dt}\,\tau+\xi(t,\tau)\Bigg],
\end{aligned} \tag{18}$$

where

$$\xi(t,\tau)=\sum_{l=q/2}^{(p-1)/2}\frac{\tau^{(2l+1)}}{(2l+1)!}\,\frac{d^{(2l+1)}\phi(t)}{dt^{(2l+1)}}\sum_{k=-q/2}^{q/2} b_k c_k^{(2l+1)}. \tag{19}$$

In the above expansion we have made use of the fact that the c_k and b_k coefficients of the qth-order polynomial Wigner–Ville kernel are chosen such that the coefficients of $[d^n\phi(t)/dt^n]\tau^n$ are zero for $1<n<q$ and unity for $n=1$.[15]

Using the above kernel expansion, the qth-order polynomial Wigner–Ville distribution (6) can be expressed as

$$W_q(t,f) = \int_{-\infty}^{\infty} h(\tau)\exp\left\{ j2\pi\left[\left(\frac{d\phi(t)}{dt} - f\right)\tau + \xi(t,\tau)\right]\right\} d\tau$$
$$= \int_{-T/2}^{T/2} \exp\left\{ j2\pi\left[\left(\frac{d\phi(t)}{dt} - f\right)\tau + \xi(t,\tau)\right]\right\} d\tau \tag{20}$$

with a rectangular window $h(\tau)$ of length T.

The instantaneous frequency estimate $\hat{f}_i(t)$ is then determined by the peak of (20) so that

$$\hat{f}_i(t) \triangleq \underset{f}{\text{argmax}}\{|W_q(t,f)|\}, \tag{21}$$

where f is an element of the set of real numbers. By the stationary phase principal,[18] the abscissa(s) of the frequency peak(s) of the polynomial Wigner–Ville distribution are approximately given by the values of f, at each instant of time, for which the phase of the integrand of (20) is stationary, or equivalently, where the first derivative of the kernel phase, with respect to τ, is zero.

$$\frac{\partial}{\partial\tau}\left[\left(\frac{d\phi(t)}{dt} - \hat{f}_i(t)\right)\tau + \xi(t,\tau)\right] \equiv 0. \tag{22}$$

Thus for the polynomial Wigner–Ville peak-based instantaneous frequency estimator,

$$\hat{f}_i(t) = \frac{d\phi(t)}{dt} = \frac{\partial\xi(t,\tau)}{\partial\tau}. \tag{23}$$

From (5), $d\phi(t)/dt$ is defined as the true instantaneous frequency $f_i(t)$ of the signal $s(t)$ and so the systematic bias $\epsilon(t)$ can be explicitly written as

$$\epsilon(t) = \hat{f}_i(t) - f_i(t)$$
$$= \frac{\partial\xi(t,\tau)}{\partial\tau}$$
$$= \sum_{l=q/2}^{(p=1)/2} \frac{\tau^{2l}}{(2l)!}\frac{d^{(2l+1)}\phi(t)}{dt^{(2l+1)}} \sum_{k=-q/2}^{q/2} b_k c_k^{(2l+1)} \tag{24}$$

with the maximum value of $\tau = T/2$. Equivalently, for the discrete time polynomial Wigner–Ville distribution with rectangular window of length L and sampling frequency f_s, the maximum value of $\tau = L/(2f_s)$. From (24) it can be seen that the higher-order derivatives of the signal phase in (18) (i.e., $d^n\phi/dt^n$, $n > q$) will generally introduce an error in the instantaneous frequency estimator. These higher-order components are due solely to the phase order mismatch between the signal and the polynomial Wigner–Ville kernel. In practice, due to the factorial denominator in (24) and the often decreasing value of higher-order phase derivatives, $\epsilon(t)$ may be dominated by the first term in the summation in l. In this case, and by making the substitution $\tau = L/(2f_s)$, the maximum systematic bias is approximately

$$\epsilon(t) \approx \frac{L^q}{(2f_s)^q q!}\frac{d^{(q+1)}\phi(t)}{dt^{(q+1)}} \sum_{k=-q/2}^{q/2} b_k c_k^{(q+1)}. \tag{25}$$

This result confirms our previous observation that the systematic bias can be controlled via the length of the window function $h(\tau)$ by effectively restricting the possible excursion on τ in (18). As we may expect, in considering only the systematic bias of the unmatched polynomial Wigner–Ville distribution, the window length should be chosen as small as possible so as to reduce the effect of the error term $\epsilon(t)$. Equation (24) [or (25), as appropriate] provides the first step in deriving an expression for the mean-square error of the polynomial Wigner–Ville-based instantaneous frequency estimator. We next require an expression for the estimator variance.

D. Polynomial Wigner–Ville-based instantaneous frequency estimator variance

The polynomial Wigner–Ville distribution, as defined by (6) is the Fourier transform of the kernel function $K(t,\tau)$. As previously discussed, this kernel function attempts to resolve a nonstationary signal, at each time instant, into a sinusoid having frequency given by the instantaneous frequency. Thus, in considering the usual discrete time implementation, the analysis of variance of $\hat{f}_i(t)$ reduces to that associated with estimating the frequency of a discrete noisy sinusoid from the peak of the magnitude of the discrete Fourier transform (DFT). The point to note here is that, due to the multilinear nature of $K(t,\tau)$, the signal-to-noise ratio (denoted $\mathscr{S}_K$) of the noisy kernel sinusoid will be less than the signal-to-noise ratio of the original signal under analysis. In this section we derive an expression for $\mathscr{S}_K$ leading to an expression for the variance of $\hat{f}_i(t)$.

For the case of the peak of the magnitude of the discrete Fourier transform of a discrete noisy sinusoid of length N with constant scale A, unknown initial phase, and for sufficiently high signal-to-noise ratio (specifically, above a threshold value to be described in Sec. III D 1) and for all but very small values of N, the frequency estimator variance $\text{var}_{\text{DFT}}(\hat{f})$ closely approximates the Cramér–Rao lower bound.[17,19]

$$\text{var}_{\text{DFT}}(\hat{f}) = \frac{12 f_s^2}{(2\pi)^2 \mathscr{S}(N^2-1)N}, \tag{26}$$

where

$$\mathscr{S} = A^2/\sigma^2 \tag{27}$$

and σ^2 is the variance of the real noise. Based on this result, to determine the variance of the polynomial Wigner–Ville peak-based instantaneous frequency estimator, it only remains to determine the signal-to-noise ratio of the polynomial Wigner–Ville kernel. Consider the complex signal

$$z(t) = s(t) + n(t), \tag{28}$$

where $s(t)$ has been previously defined in (16) and $n(t)$ is a zero-mean, complex independent white Gaussian stationary noise process with variance $\text{var}[n(t)] = \text{var}[n_{\mathscr{R}}(t)] + \text{var}[n_{\mathscr{I}}(t)] = \sigma^2 + \sigma^2 = 2\sigma^2$, where $n_{\mathscr{R}}(t)$ and $n_{\mathscr{I}}(t)$ are the real and imaginary noise components, respectively.

To formulate an expression for the kernel signal-to-noise ratio we begin by considering the expansion of the qth-order polynomial Wigner–Ville kernel (7) for the signal $z(t)$.

$$
\begin{aligned}
&K_q(t,\tau)\\
&\quad=\prod_{k=1}^{q/2}\,[s(t+c_k\tau)+n(t+c_k\tau)]^{b_k}\\
&\qquad\times[s^*(t+c_{-k}\tau)+n^*(t+c_{-k}\tau)]^{b_k}\\
&\quad=\prod_{k=1}^{q/2}\left\{\left[\sum_{j=0}^{b_k}\binom{b_k}{j}n^j(t+c_k\tau)s^{b_k-j}(t+c_k\tau)\right]\right.\\
&\qquad\left.\times\left[\sum_{m=0}^{b_k}\binom{b_k}{m}n^{*m}(t+c_{-k}\tau)s^{*(b_k-m)}(t+c_{-k}\tau)\right]\right\}\\
&\quad=\prod_{k=1}^{q/2}\{[s^{b_k}(t+c_k\tau)+b_ks^{b_k-1}(t+c_k\tau)n(t+c_k\tau)+\cdots]\\
&\qquad\times[s^{*b_k}(t+c_{-k}\tau)+b_ks^{*(b_k-1)}(t+c_{-k}\tau)\\
&\qquad\times n^*(t+c_{-k}\tau)+\cdots]\},
\end{aligned}
\tag{29}
$$

and finally

$$
\begin{aligned}
K_q(t,\tau)=&\prod_{k=1}^{q/2}\,s^{b_k}(t+c_k\tau)s^{*b_k}(t+c_{-k}\tau)\\
&+\left[\prod_{k=1}^{q/2}\,s^{b_k}(t+c_k\tau)s^{*b_k}(t+c_{-k}\tau)\right]\\
&\times\left\{\sum_{j=1}^{q/2}\,b_j[s^{-1}(t+c_j\tau)n(t+c_j\tau)\right.\\
&\left.+s^{*-1}(t+c_{-j}\tau)n^*(t+c_{-j}\tau)]+\cdots\right\}\\
&+\prod_{k=1}^{q/2}\,n^{b_k}(t+c_k\tau)n^{*b_k}(t+c_{-k}\tau),
\end{aligned}
\tag{30}
$$

where the asterisk denotes complex conjugation. This results generalizes the result in Ref. 20.

This expansion reveals three types of terms: a signal self-term [first line of (30)], a noise self-term [last line of (30)], and signal–noise cross terms [the remaining terms in (30)]. First, the term containing only signal terms is simply the expression for the qth-order PWVD kernel of the noiseless signal $s(t)$. The amplitude of this term is A^{b_Σ}, where

$$
b_\Sigma=\sum_{k=-q/2}^{q/2}|b_k|=2\sum_{k=1}^{q/2}|b_k| \tag{31}
$$

and consequently has power

$$
P_S=A^{2b_\Sigma}. \tag{32}
$$

Second, the term containing only noise terms has power

$$
P_{\mathrm{N}}=\begin{cases}\Pi_{k=0}^{q/2}\mathbb{U}_{2b_k} & \text{if } \tau\neq 0,\\ \mathbb{U}_{2b_\Sigma} & \text{if } \tau=0,\end{cases} \tag{33}
$$

where $\mathbb{U}_p$ is the pth moment of $|n(t)|$

$$
\begin{aligned}
\mathbb{U}_p&=E(|n(t)|^p)\\
&=E[(n_{\mathscr{R}}(t)^2+n_{\mathscr{I}}(t)^2)^{p/2}]\\
&=\sum_{i=0}^{p/2}\binom{p/2}{i}E(n_{\mathscr{R}}(t)^{(p-2i)})E(n_{\mathscr{I}}(t)^{(2i)})\\
&=\sum_{i=0}^{p/2}\binom{p/2}{i}\mu_{(p-2i)}\mu_{2i},
\end{aligned}
\tag{34}
$$

where $\mu_n=1\cdot3\cdot5\cdot\cdots\cdot(n-1)\sigma^n$ and $E(\cdot)$ is the expectation operator.

Third, at high signal-to-noise ratio, the signal–noise cross terms are dominated by the terms in the expansion which are a product of a single-noise term and $(b_\Sigma-1)$ signal terms. Consequently the cross terms indicated as $+\cdots$ in (30) will be neglected.

For each $j=1\cdots q/2$, the power of the cross terms is

$$
(b_jA^{b_\Sigma-1})^2 2\sigma^2=2b_j^2A^{2(b_\Sigma-1)}\sigma^2 \tag{35}
$$

and the total cross term power can be approximated as

$$
P_{\mathrm{SN}}\approx 2\sum\,b^2A^{2(b_\Sigma-1)}\sigma^2, \tag{36}
$$

where

$$
\sum\,b^2=\sum_{k=-q/2}^{q/2}b_k^2. \tag{37}
$$

Comparing P_{N} and P_{SN} at high signal-to-noise ratio, it can be seen that the total noise power $(P_{\mathrm{N}}+P_{\mathrm{SN}})$ will be dominated by the P_{SN} term. We can therefore conclude that the signal-to-noise ratio of the polynomial Wigner–Ville kernel will be lower than the signal-to-noise ratio of $z(t)$ due to the signal–noise cross terms generated by the multilinear kernel. The kernel signal-to-noise ratio is approximately:

$$
\mathscr{S}_K\approx\frac{P_{\mathrm{S}}}{P_{\mathrm{SN}}}=\frac{A^2}{2\Sigma b^2\sigma^2}=\frac{\mathscr{S}}{2\Sigma b^2}. \tag{38}
$$

In addition, the effective length of the signal is reduced by the conjugate symmetry of the kernel such that $N=L/2$.[21] Thus from (26), the polynomial Wigner–Ville-based instantaneous frequency estimator variance is approximately given by

$$
\mathrm{var}_{\mathrm{PWVD}}(\hat{f}\,)\approx\frac{12\Sigma b^2\sigma^2f_s^2}{(2\pi)^2A^2[(L^2/4)-1]L/2}. \tag{39}
$$

This result confirms that the longer the window length L at a given signal-to-noise ratio, the lower the variance of the instantaneous frequency estimator. As we may expect, in considering variance stability alone, the window length should be as long as possible. Equation (39) provides the variance

term in the expression for the mean-square error of the polynomial Wigner–Ville-based instantaneous frequency estimator. In deriving expressions for both the bias (24) and variance (39) we have assumed high signal-to-noise ratio. We show in the next section that the polynomial Wigner–Ville-based instantaneous frequency estimator is subject to a signal-to-noise ratio threshold beyond which the estimator variance increases dramatically. In practice therefore, the polynomial Wigner–Ville distribution (including the Wigner–Ville distribution) is used at signal-to-noise ratio levels above the threshold and thus the high signal-to-noise ratio assumption is reasonable.

1. Polynomial Wigner–Ville-based instantaneous frequency estimator variance threshold

The derivation of the variance of the polynomial Wigner–Ville-based instantaneous frequency estimator (39) was based on the result for the variance of the frequency estimator based on the peak of the magnitude of the discrete Fourier transform under the assumption of high signal-to-noise ratio. For fixed data length N and decreasing signal-to-noise ratio, or for fixed signal-to-noise ratio and decreasing data length, the variance is known to reach a threshold $\mathscr{S}_{\mathrm{THRES}}$ beyond which the variance increases dramatically.[19] This result can be directly applied to the polynomial Wigner–Ville distribution which is the discrete Fourier transform of the kernel $K(t,\tau)$ in the variable τ. Quinn and Kootsookos[19] showed that the signal-to-noise ratio at which this threshold occurs can be approximated (quite accurately) as

$$\psi_D = 10\log_{10}\{[6\log(N)+2\log(\log(N))+4\log(\pi) - 2\log(6)]/(N-1)\}\ \text{dB}. \tag{40}$$

From (38), $\mathscr{S}\approx\mathscr{S}_K 2\Sigma b^2$ and rearranging in terms of the original signal-to-noise ratio $\mathscr{S}=A^2/\sigma^2$, and making the substitution $N=L/2$ yields

$$\mathscr{S}_{\mathrm{THRES}} = 10\log_{10}\left\{\frac{2\Sigma b^2}{(L/2-1)}\,[6\log(L/2) + 2\log(\log(L/2))+4\log(\pi) - 2\log(6)]\right\}\ \text{dB}, \tag{41}$$

which provides a lower signal-to-noise ratio bound for the approximation in (39). From (41) it can be seen that the $\mathscr{S}_{\mathrm{THRES}}$ for the Wigner–Ville distribution ($\Sigma b^2=2$) will be approximately 7 dB lower than for the fourth-order polynomial Wigner–Ville distribution ($\Sigma b^2=10$). For this reason the use of the polynomial Wigner–Ville distribution is restricted to applications having sufficiently high signal-to-noise ratio.

E. Polynomial Wigner–Ville optimal window length

Using the expression for the bias (24) and variance (39), the mean-square error $\lambda(L)$ of the qth-order polynomial Wigner–Ville-based instantaneous frequency estimator at a given signal-to-noise ratio (above the threshold) can be expressed as

$$\lambda(L) = \frac{12\Sigma b^2 f_s^2}{(2\pi)^2\mathscr{S}[(L^2/4)-1]L/2} + \left[\sum_{l=q/2}^{(p-1)/2} \frac{L^{2l}}{(2f_s)^{2l}(2l)!}\frac{d^{(2l+1)}\phi(t)}{dt^{(2l+1)}} \times \sum_{k=-q/2}^{q/2} b_k c_k^{(2l+1)}\right]^2 \tag{42}$$

and by using the simplified bias expression of (25), $\lambda(L)$ can, where appropriate, be approximated as

$$\lambda(L) \approx \frac{12\Sigma b^2 f_s^2}{(2\pi)^2\mathscr{S}[(L^2/4)-1]L/2} + L^{2q}\left[\frac{1}{(2f_s)^q q!}\frac{d^{(q+1)}\phi(t)}{dt^{(q+1)}}\sum_{k=-q/2}^{q/2} b_k c_k^{(q+1)}\right]^2. \tag{43}$$

A minimum mean-square error, assuming one exists, can be found by setting

$$\frac{\partial\lambda(L)}{\partial L}=0, \tag{44}$$

which yields

$$a\,\frac{(3L^2-4)}{(L^3-4L)^2} = L^{(2q-1)}b, \tag{45}$$

where

$$a = \frac{96\Sigma b^2 f_s^2}{(2\pi)^2\mathscr{S}}, \tag{46}$$

$$b = 2^{2q}\left(\frac{1}{(2f_s)^q q!}\frac{d^{(q+1)}\phi(t)}{dt^{(q+1)}}\sum_{k=-q/2}^{q/2} b_k c_k^{(q+1)}\right)^2. \tag{47}$$

Rearranging yields

$$L^{2q-1}(L^6-4L^4+16L^2) = (3L^2-4)a/b \tag{48}$$

for which an approximate solution, for $L\gg 1$, is given by

$$L\approx\left(\frac{3a}{b}\right)^{1/(2q+3)}. \tag{49}$$

Thus in (49) we have achieved the objective of this section to derive an expression for the window length L which minimizes the mean-square error of the qth-order polynomial Wigner–Ville-based instantaneous frequency estimator. In deriving this result, a number of simplifying assumptions have been made and it is not readily apparent what combined effect this has on the result. In the next section we establish the practical usefulness of (49) by applying the optimal window theory to simulated data.[3]

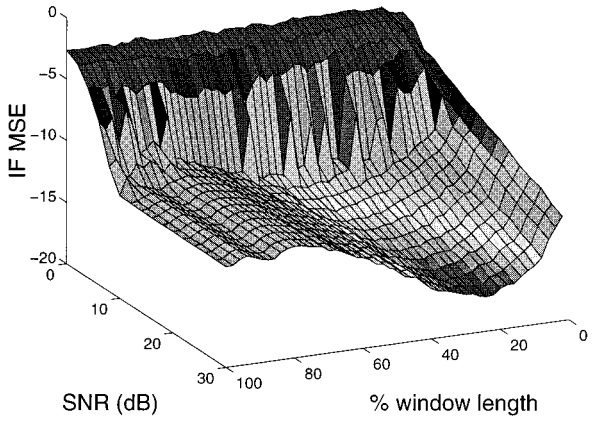

FIG. 19. Instantaneous frequency estimator mean-square error for a fifth-order polynomial phase signal for varying signal-to-noise ratio and window length. The instantaneous frequency was estimated from the peak of the fourth-order polynomial Wigner–Ville distribution calculated at the central time instant ($t=0$).

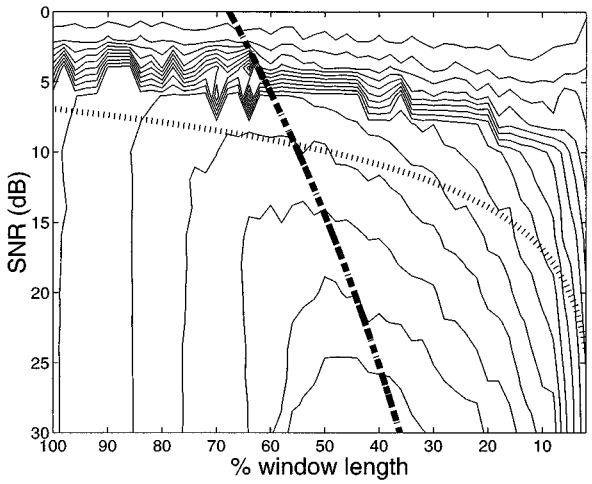

FIG. 20. A contour plot of the mean-square error surface of Fig. 19. The heavy dashed line represents the theoretical line of minimum mean-square error calculated using Eq. (49). The finer broken line represents the theoretical variance threshold calculated using Eq. (41).

IV. EXAMPLES

A. Instantaneous frequency estimator minimum mean-square error

In the previous section we derived an expression for the polynomial Wigner–Ville window length which yielded the instantaneous frequency estimator minimum mean-square error. This result is now verified by computer simulation.

In these examples we estimate the instantaneous frequency of a fifth-order polynomial phase test signal using the fourth-order polynomial Wigner–Ville distribution. The polynomial order of the test signal is intentionally chosen to be higher than that of the time–frequency representation so that the optimal window theory can be applied. The test signal $z(t)$ is of the form (28).

1. Example 1

In the first simulation the phase of $z(t)$ is chosen to be

$$\phi(t)=0.25t+\frac{0.25t^5}{5(64^4)},$$

$$t=-N/2+1,\ldots,N/2-1, \quad N=128. \tag{50}$$

Using the fourth-order polynomial Wigner–Ville distribution, the instantaneous frequency was estimated for signal-to-noise ratio values of 0,2,4,...,30 dB and window length $L=2,4,6,\ldots,100$ as a percentage of the total data length. The estimator mean-square error was then computed from 200 realizations. So that the full range of window lengths could be used, it was necessary to calculate the mean-square error at the central time instant (i.e., $t=0$) as this is the only point where a full length window could be applied. The mean-square error surface for this experiment is shown in Fig. 19 where a *valley* of minimum mean-square error can be clearly seen. Figure 20 shows a contour plot of the same mean-square error surface. The heavy dashed line represents the theoretical line of minimum mean-square error calculated from (49) and is closely aligned with the empirical result. The variance threshold effect, as discussed in Sec. III D 1, is also apparent in Fig. 20 where the finer broken line represents the theoretical variance threshold as predicted by (41).

2. Example 2

In this second simulation, the phase of $z(t)$ (50) is modified so as to reduce the coefficient of the fifth derivative of phase.

$$\phi(t)=\frac{0.5t^5}{5(128^4)}, \quad t=0,1,2,\ldots,N-1, \quad N=128. \tag{51}$$

The mean-square error surface for this experiment, calculated at the central time instant $t=64$, is shown in Fig. 21. It can be seen that, due to the lower value of the fifth derivative, the minimum mean-square error occurs for larger window lengths than for example 1. The theoretical minimum mean-square error, calculated from (49), is shown in the contour plot of Fig. 22 and again it is closely aligned with the

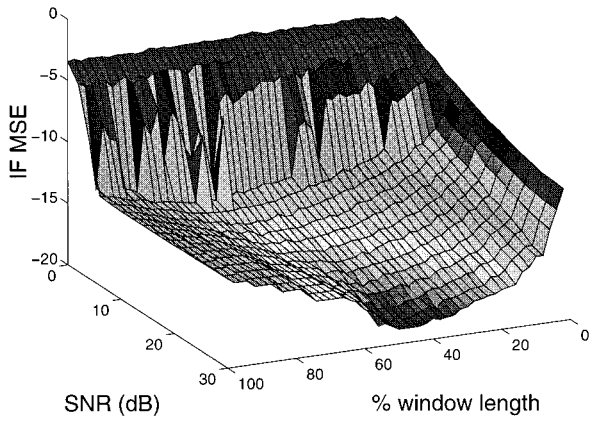

FIG. 21. Instantaneous frequency estimator mean-square error for a fifth-order polynomial phase signal for varying signal-to-noise ratio and window length. For the test signal used in this example, the fifth derivative of phase is less than for the test signal used in Fig. 19. The instantaneous frequency was estimated from the peak of the fourth-order polynomial Wigner–Ville distribution calculated at the central time instant ($t=64$).

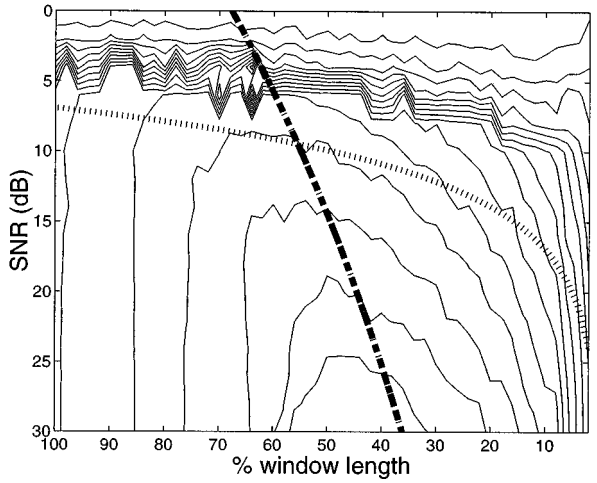

FIG. 22. A contour plot of the mean-square error surface of Fig. 21. The heavy dashed line represents the theoretical line of minimum mean-square error calculated using Eq. (49). The finer broken line represents the theoretical variance threshold calculated using (41).

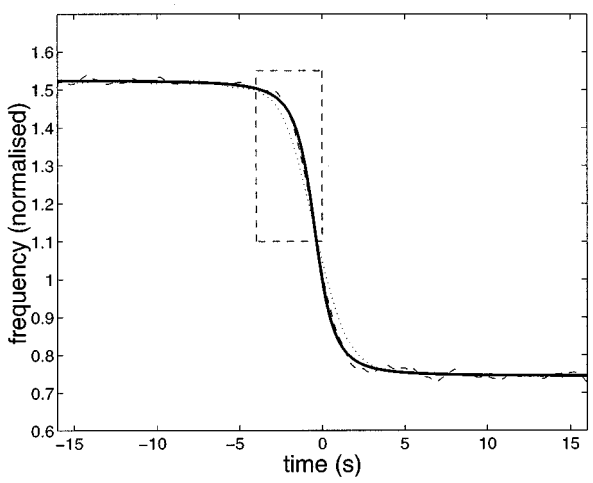

FIG. 23. A comparison of the Wigner–Ville (dotted line) and polynomial Wigner–Ville (dashed line) based instantaneous frequency estimates of a simulated passive acoustic signal at 20-dB signal-to-noise ratio. The true instantaneous frequency (solid line) represents an aircraft with the following parameters: $h=152.4$ m (500 ft), $v=30.8$ m/s (60 kn), $r=1.837$ km and normalized source frequency.

empirical result. The finer broken line represents the theoretical variance threshold as predicted by (41) and, as this threshold is not signal dependent, is unchanged from the previous example.

B. Passive acoustic parameter estimation

We now return to our original focus of passive acoustic parameter estimation. In the first experiment we use a real passive acoustic recording to demonstrate the importance of using the correct window length in estimating the aircraft flight parameters. In experiments 2–4 passive acoustic signals are synthesized using the observer frequency model (2) with chosen parameters and with additive stationary, white Gaussian noise. The sample mean and variance for the Wigner–Ville- and fourth-order polynomial Wigner–Ville-based estimators are then computed over multiple realizations so as to evaluate the relative performance of these two estimation schemes. These examples demonstrate that, by using the optimal window, the fourth-order polynomial Wigner–Ville distribution will yield flight parameter estimates having lower mean-square error than for the Wigner–Ville distribution (second-order polynomial Wigner–Ville distribution) in the high signal-to-noise ratio case.

1. Experiment 1

In Sec. II C a recording of an overflying aircraft was analyzed separately using the Wigner–Ville distribution and fourth-order polynomial Wigner–Ville distribution to estimate the aircraft's physical parameters. The time–frequency representations, and the resulting aircraft parameter estimates of Table I, were calculated using a 30% window. To demonstrate the influence of the window length, the aircraft parameters are recalculated in Table II using a larger window (50%) and shorter window (15%) and are compared to those estimated in Table I (30% window).

In this example the estimates were based on a single recording and so it is not possible to draw any conclusions as to the relative merit of each of the estimators. However, it does serve to demonstrate the importance of choosing the correct window length when applying the polynomial Wigner–Ville distribution (thus including the Wigner–Ville distribution) to the passive acoustic problem. More quantitative results are provided using synthesized passive acoustic data in the following examples.

2. Experiment 2

In this example we use a synthesized signal (144 data points, sampling frequency $f_s=4$ Hz) representative of an overflying aircraft at 20-dB signal-to-noise ratio with the following parameters: $h=152.4$ m (500 ft), $v_a=30.8$ m/s (60 kn), $r=1.837$ km, and normalized source frequency. The observer frequency model for this signal, which is shown in Fig. 23 (solid line), exhibits a sharp transition between the maximum and minimum Doppler shifted frequencies. The

TABLE II. Comparison of aircraft flight parameter estimates from real passive acoustic data using the Wigner–Ville and fourth-order polynomial Wigner–Ville distribution where a 50% (bold face), 15% (italicized), and 30% (bracketed) window length has been used.

	Height (m)	Velocity (m/s)	Range (km)	Source freq. (Hz)
WVD	**897** *334* (404)	**87.8** *71.0* (73.3)	**1.70** *1.25* (1.30)	**66.2** *68.6* (68.4)
PWVD	**383** *301* (309)	**71.0** *67.6* (68.7)	**1.26** *1.17* (1.21)	**68.5** *69.0* (68.9)

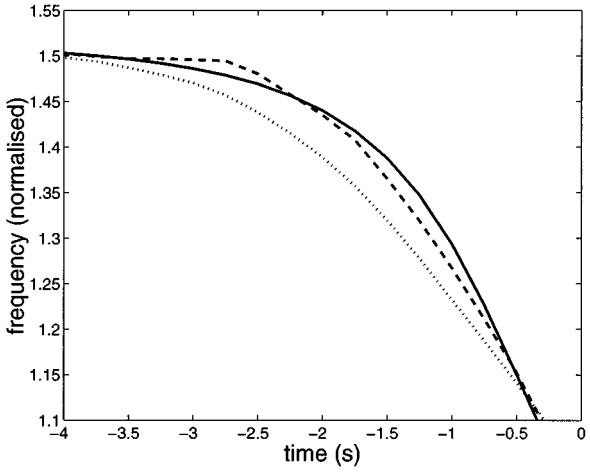

FIG. 24. An enlarged portion of Fig. 23 (in the region marked by the dashed rectangular box) which shows, for a typical realization, the departure of the Wigner–Ville-based (dotted line) and polynomial Wigner–Ville-based (dashed line) instantaneous frequency estimates from the true instantaneous frequency (solid line).

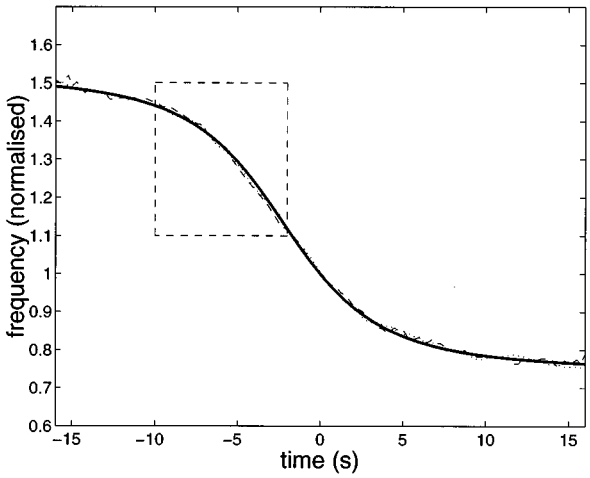

FIG. 25. A comparison of Wigner–Ville-based (dotted line) and polynomial Wigner–Ville-based (dashed line) instantaneous frequency estimates of a simulated passive acoustic signal at 12-dB signal-to-noise ratio. The true instantaneous frequency (solid line) represents an aircraft with the following parameters: $h=762.0$ m (2500 ft), $v=30.8$ m/s (60 kn), $r=1.837$ km and normalized source frequency.

coefficients of $d^3\phi(t)/dt^3$ and $d^5\phi(t)/dt^5$ for this instantaneous frequency law were estimated to be -0.07 and -9.3×10^{-4} and the optimal window length for the Wigner–Ville distribution and fourth-order polynomial Wigner–Ville distribution were computed using (49) to be 10% and 25%, respectively. From (43) the instantaneous frequency estimator mean-square error is predicted to be smaller for the fourth-order polynomial Wigner–Ville than for the Wigner–Ville distribution.

The Wigner–Ville and fourth-order polynomial Wigner–Ville-based instantaneous frequency estimates for this signal are also shown in Fig. 23 (dotted line for Wigner–Ville and dashed line for polynomial Wigner–Ville) and more clearly in Fig. 24 for the region marked by the dashed rectangular box in Fig. 23. The sample mean, variance, and mean-square error of the aircraft flight parameter estimates, based on 50 realizations of this signal, are given in Table III.

Considering the estimator mean-square error in Table III, these results demonstrate the superior performance of the fourth-order polynomial Wigner–Ville-based flight parameter estimation method for the particular case where there is a rapid transition in the instantaneous frequency (corresponding to a high velocity and/or low altitude aircraft) and where the signal-to-noise ratio is above the threshold (41).

3. Experiment 3

In this example, the signal is the same as in example 2 except that the signal-to-noise ratio is reduced to 12 dB and the height parameter is increased to 762.0 m (2500 ft). This increase in height is reflected in a more gradually varying observer frequency model as shown in Fig. 25 (solid line). The coefficients of $d^3\phi(t)/dt^3$ and $d^5\phi(t)dt^5$ for this instantaneous frequency law were estimated to be -0.01 and -1.9×10^{-4} and the optimal window length for the Wigner–Ville and fourth-order polynomial Wigner–Ville distribution were computed using (49) to be 19% and 39%, respectively. From (43) the instantaneous frequency estimator mean-square error is predicted to be larger for the fourth-order polynomial Wigner–Ville than for the Wigner–Ville distribution.

Typical instantaneous frequency estimates for this signal are also shown in Fig. 25 (dotted line for the Wigner–Ville and dashed line for polynomial Wigner–Ville distribution).

TABLE III. Comparison of the actual aircraft flight parameter values with the sample mean and variance of the Wigner–Ville- and fourth-order polynomial Wigner–Ville-based flight parameter estimators. The deterministic instantaneous frequency law for this simulated signal is shown in Fig. 23. These statistics were computed from 50 realizations using simulated passive acoustic data at 20-dB signal-to-noise ratio.

	Height (m)		Velocity (m/s)		Range (km)		Source freq. (norm)	
	mean	variance	mean	variance	mean	variance	mean	variance
Actual	152.4		30.8		1.837		1	
WVD	227.3	7.08	31.3	0.001	1.889	9.31×10^{-6}	0.996	1.718×10^{-7}
$PWVD_4$	154.3	20.26	31.1	0.003	1.854	3.14×10^{-5}	0.998	7.442×10^{-7}
	Estimated MSE		Estimated MSE		Estimated MSE		Estimated MSE	
WVD	5617		0.250		27.13×10^{-4}		16.17×10^{-6}	
$PWVD_4$	23.87		0.092		3.20×10^{-4}		4.74×10^{-6}	

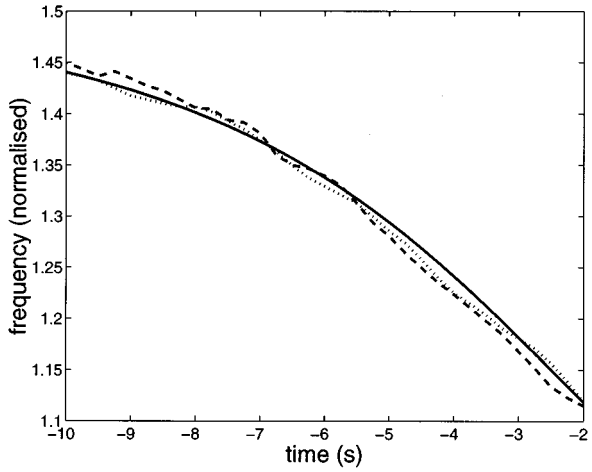

FIG. 26. An enlarged portion of Fig. 25 (in the region marked by the dashed rectangular box) which shows, for a typical realization, the departure of the Wigner–Ville-based (dotted line) and polynomial Wigner–Ville-based (dashed line) instantaneous frequency estimates from the true instantaneous frequency (solid line).

The region of Fig. 25 indicated by the dashed rectangular box is shown more clearly in the enlarged view of Fig. 26. The aircraft flight parameter estimator sample mean, variance, and mean-square error, base on 50 realizations of this signal, are given in Table IV.

It is clear from Table IV that the Wigner–Ville distribution has performed better than the fourth-order polynomial Wigner–Ville distribution. This result is predicted by (43) and demonstrates that, while the bias of the polynomial Wigner–Ville-based estimator is always less than that of the Wigner–Ville distribution, the greater variance of the polynomial Wigner–Ville distribution, at reduced signal-to-noise ratio, may result in higher estimator mean-square error.

4. Experiment 4

In our final example, the aircraft flight parameters are unchanged from example 3 and the signal-to-noise ratio is increased to 20 dB. The optimal window length for the Wigner–Ville and fourth-order polynomial Wigner–Ville distribution were computed using (49) to be 13% and 22%, respectively. The flight parameter estimator sample mean, variance, and mean-square error, based on 50 realizations of this signal, are given in Table V. In this example, where the signal-to-noise ratio is high, the polynomial Wigner–Ville-based estimator has performed better than the Wigner–Ville distribution. As predicted by (43), the improvement is not as great as in the first example (Table III) where the coefficient of $d^3\phi(t)/dt^3$ was higher.

5. Discussion of results

The previous four experiments demonstrated the following points. Experiment 1 showed that the flight parameter estimates are very much dependent on the chosen window length. The optimal window theory allows us to find the best (in the minimum mean-square error sense) estimators. Experiment 2 demonstrated that the flight parameter estimator based on the fourth-order polynomial Wigner–Ville distribution is better (again in the minimum mean-square error sense) than that based on the Wigner–Ville distribution when the signal-to-noise ratio is above the threshold. The more rapid the transition in the instantaneous frequency [in particular, the higher the coefficient of $d^3\phi(t)/dt^3$] the better the performance of the polynomial Wigner–Ville relative to the Wigner–Ville distribution [see Eq. (42)]. In experiment 3, the relative performance of the polynomial Wigner–Ville distribution is reduced by two factors; first, the instantaneous frequency is slowly varying, and second the signal-to-noise ratio has been reduced. The result is that, under these conditions, the Wigner–Ville distribution has performed better than the polynomial Wigner–Ville distribution. However, example 4 shows that even for a slowly varying instantaneous frequency, the fourth-order polynomial Wigner–Ville distribution performs better than the Wigner–Ville distribution at high signal-to-noise ratio.

In this paper, we have considered a frequency model which assumes straight, level, and constant velocity flight throughout the observation period. Other more complex models may be proposed. For example, it has been suggested[22] that the observer frequency model for an aircraft in a distant (not directly overhead) circular flight path would be of an oscillatory form and therefore highly nonlinear. Because such a flight parameter estimation scheme would necessitate the estimation of higher-order instantaneous frequency laws, the use of the polynomial Wigner–Ville may be particularly appropriate.

TABLE IV. Comparison of the actual aircraft flight parameter values with the sample mean and variance of the Wigner–Ville- and fourth-order polynomial Wigner–Ville-based flight parameter estimators. The deterministic instantaneous frequency law for this simulated signal is shown in Fig. 25. These statistics were computed from 50 realizations using simulated passive acoustic data at 12-dB signal-to-noise ratio.

	Height (m)		Velocity (m/s)		Range (km)		Source freq. (norm)	
	mean	variance	mean	variance	mean	variance	mean	variance
Actual	762.0		30.8		1.837		1	
WVD	790.3	1040	31.0	0.098	1.854	7.46×10^{-4}	0.999	6.27×10^{-6}
$PWVD_4$	792.5	3140	31.1	0.312	1.867	3.35×10^{-3}	0.997	3.04×10^{-5}
	Estimated MSE		Estimated MSE		Estimated MSE		Estimated MSE	
WVD	1841		0.14		1.03×10^{-3}		7.3×10^{-6}	
$PWVD_4$	4070		0.40		4.25×10^{-3}		39.4×10^{-6}	

TABLE V. Comparison of the actual aircraft flight parameter values with the sample mean and variance of the Wigner–Ville- and fourth-order polynomial Wigner–Ville-based flight parameter estimators. The deterministic instantaneous frequency law for this simulated signal is shown in Fig. 25. These statistics were computed from 50 realizations using simulated passive acoustic data at 20-dB signal-to-noise ratio.

	Height (m)		Velocity (m/s)		Range (km)		Source freq. (norm)	
	mean	variance	mean	variance	mean	variance	mean	variance
Actual	762.0		30.8		1.837		1	
WVD	774.8	125.4	30.9	0.026	1.845	1.05×10^{-4}	0.9995	9.39×10^{-7}
$PWVD_4$	765.6	129.1	30.9	0.026	1.841	1.09×10^{-4}	0.9997	1.04×10^{-6}
	Estimated MSE		Estimated MSE		Estimated MSE		Estimated MSE	
WVD	289.2		0.036		3.94×10^{-4}		1.19×10^{-6}	
$PWVD_4$	142.0		0.036		1.25×10^{-4}		1.13×10^{-6}	

V. CONCLUSION

The sound from an overflying aircraft, as heard by a stationary observer, can be used to estimate the aircraft's flight parameters. This passive acoustic approach is demonstrated using an observer frequency model to describe the time varying acoustic Doppler shift. Central to the success of this frequency-based passive acoustic flight parameter estimation scheme is the need for an accurate estimate of the time varying instantaneous frequency. We have considered the Wigner–Ville distribution (second-order polynomial Wigner–Ville distribution) and the generalized qth-order polynomial Wigner–Ville distribution in this application. We have shown that instantaneous frequency estimators based on the peak of the windowed polynomial Wigner–Ville distribution are subject to two error factors which behave in a counterdependent manner over the time domain window length. The first, which is due to the systematic bias, is a result of a mismatch between the polynomial order of the polynomial Wigner–Ville distribution and the phase of the signal under analysis. The second error is due to the variance of the estimator.

An expression is derived for the window length which minimizes the estimator mean-square error, as a function of signal-to-noise ratio and the coefficients of the higher-order derivatives of the signal phase. This general theoretical result is then applied to the passive acoustic aircraft flight parameter estimation problem where it was shown, using computer simulations, that the fourth-order polynomial Wigner–Ville-based estimator can provide a lower mean-square error than the more commonly used Wigner–Ville distribution. This is particularly the case for signals at high signal-to-noise ratio having rapidly changing instantaneous frequency such as occur for aircrafts at low altitude. For signals at low signal-to-noise ratio having slowly changing instantaneous frequency such as occur for high altitude aircraft, the polynomial Wigner–Ville distribution may provide little or no improvement.

The observer frequency model employed in this paper assumes that the aircraft flight parameters are constant throughout the observation period. Other more complex models could be considered in future research. Such models may necessitate the estimation of higher-order instantaneous frequency laws and the use of the polynomial Wigner–Ville distribution may therefore be particularly appropriate.

ACKNOWLEDGMENTS

The authors acknowledge Jonathon Ralston for his earlier contribution to this work.[16] The authors would like to thank the anonymous reviewers for their helpful comments, and the Australian Research Council for partial funding of this research through its mechanism B.

[1] B. Ferguson, ''A ground based narrow-band passive acoustic technique for estimating the altitude and speed of a propeller driven aircraft,'' J. Acoust. Soc. Am. **92**, 1403–1407 (1992).
[2] B. G. Ferguson and G. C. Speechley, ''Time-varying spectral analysis and spatial array processing of acoustic data from a microphone array,'' in *Proceedings of the 3rd IASTED International Symposium on Signal Processing and its Applications, ISSPA 92,* edited by B. Boashash and D. A. Gray (Gold Coast, Australia, 1992), pp. 408–411.
[3] D. C. Reid, ''Improved Aircraft Flight Parameter Estimation based on Passive Acoustic Techniques using Time-Frequency Analysis,'' Ph.D. thesis, Queensland University of Technology, 1997.
[4] B. G. Ferguson and B. G. Quinn, ''Application of the short-time Fourier transform and the Wigner–Ville distribution to the acoustic localization of aircraft,'' J. Acoust. Soc. Am. **96**, 821–827 (1994).
[5] B. G. Ferguson, R. C. Trider, and J. L. Hanlon, ''Acoustic detection, recognition, and localization of propellor-driven aircraft and helicopters,'' in *Proceedings of the Fourth International Conference on Signal Processing Applications and Technology* (Defence Science and Technology Organization, Sydney, Australia, 1993), Vol. 2, pp. 1578–1583.
[6] B. G. Ferguson, ''Doppler effect for sound emitted by a moving airborne source and received by acoustic sensors located above and below the sea surface,'' J. Acoust. Soc. Am. **94**, 3244–3247 (1993).
[7] D. C. Reid, ''The bootstrap applied to passive acoustic aircraft flight parameter estimation,'' in *Proceedings of the IEEE International Conference on Acoustics, Speech and Signal Processing, ICASSP 96, Atlanta,* 1996 (IEEE, New York, 1996).
[8] B. Quinn, ''Doppler speed and range estimation using frequency and amplitude estimates,'' J. Acoust. Soc. Am. **98**, 2560–2566 (1995).
[9] A. M. Zoubir and B. Boashash, ''The Bootstrap: Signal Processing Applications,'' IEEE Signal Process. Mag. (to appear).
[10] B. Boashash, ''Interpreting and estimating the instantaneous frequency of a signal—Part I: Fundamentals; Part II: Algorithms,'' Proc. IEEE **80**(4), 519–569 (1992).
[11] B. Boashash and P. J. O'Shea, ''Polynomial Wigner–Ville distributions and their relationship to time-varying higher order spectra,'' IEEE Trans. Signal Process **42**, (1994).
[12] L. Cohen, ''Introduction: A primer on time-frequency distributions,'' in *Time-Frequency Signal Analysis: Methods and Applications,* edited by B. Boashash (Longman, Cheshire, 1992), Chap. 1, pp. 3–42.

[13] B. Boashash and G. Jones, ''Instantaneous frequency and time-frequency distributions,'' in *Time-Frequency Signal Analysis: Methods and Applications*, edited by B. Boashash (Longman, Cheshire, 1992), Chap. 2, pp. 43–73.
[14] B. Boashash, ''Time-frequency signal analysis,'' in *Advances in Spectrum Analysis and Array Processing*, edited by S. Haykin (Prentice-Hall, Englewood Cliffs, NJ, 1991), Vol. 1, Chap. 9, pp. 418–517.
[15] B. Ristic and B. Boashash, ''Use of cross Polynomial Wigner-Ville distribution for instantaneous frequency estimation of non-linear FM signals,'' in *Proc. IEEE-SP International Symposium on Time-Frequency and Time-Scale Analysis*, Philadelphia 1994, pp. 252–255.
[16] D. C. Reid and J. C. Ralston, ''An optimum window length for the PWVD with application to passive acoustic parameter estimation,'' in *Proceedings of the IEEE International Conference on Acoustics, Speech and Signal Processing, ICASSP 94*, Vol. IV, Adelaide, Australia (IEEE, New York, 1994), pp. 313–316.
[17] D. C. Rife and R. R. Boorstyn, ''Single tone parameter estimation from discrete-time observations,'' IEEE Trans. Inf. Theory **20**, 591–598 (1974).
[18] R. Wong, *Asymptotic Approximations of Integrals* (Academic, New York, 1989).
[19] B. Quinn and P. Kootsookos, ''Threshold behavior of the maximum likelihood estimator of frequency,'' IEEE Trans. Signal Process **42**, 3291–3294 (1994).
[20] P. O'Shea, ''Detection and estimation methods for non-stationary signals,'' Ph.D. thesis, University of Queensland, 1991.
[21] P. Rao and F. J. Taylor, ''Estimation of instantaneous frequency using the Wigner distribution,'' Electron. Lett. **26**, 246–248 (1990).
[22] Anonymous (1995). A helpful suggestion from an anonymous reviewer.